Elongational-flow elaboration of blend- and Janus-type polymeric nanoparticles

Javid Abdurahim, Christophe Serra, Madeline Vauthier

Elongational-flow elaboration of blend- and Janus-type polymeric nanoparticles

Javid Abdurahim, Christophe A. Serra, Madeline Vauthier*
Université de Strasbourg, CNRS, Institut Charles Sadron UPR 22, F-67000 Strasbourg, France

Abstract
Anisotropic particles, in shape or chemistry, have raised enthusiasm since they interact with their surrounding in unique ways, leading to complex assemblies that can be used in applications ranging from energy to health. In this study, two different types of polymeric nanoparticles, blend-type with two hydrophobic polymers and Janus type with hydrophobic and hydrophilic parts were produced thanks to an emulsification elongational-flow microprocess. Particles with controlled sizes and size distribution were successfully produced in one step and the effect of material (*e.g.* polymers' composition and concentration, solvent) and process (*e.g.* flow rates, emulsification time) parameters on nanoparticles' characteristics were thoroughly studied. Particles' diameter ranged from 90 to 200 nm, depending on the aforementioned parameters.

Keywords: Polymer, Janus, nanoparticles, elongational-flow

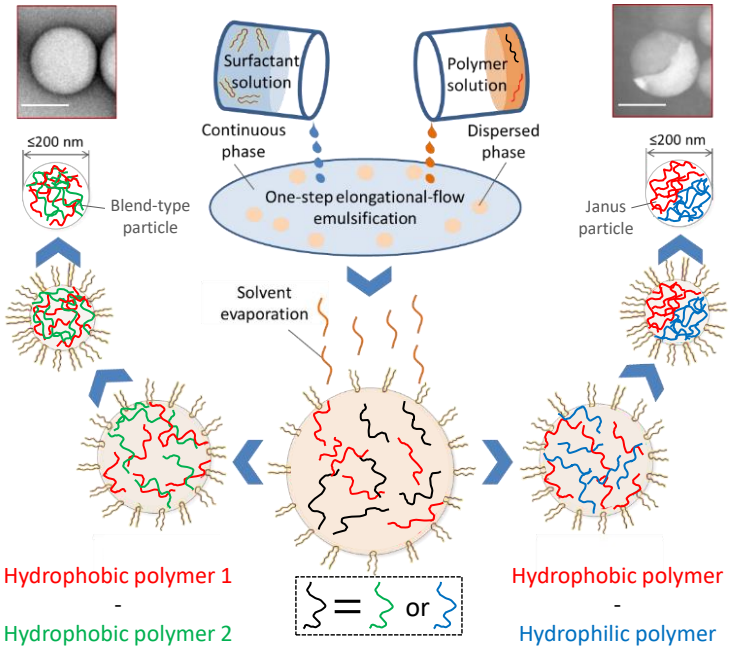

1. Introduction

Nanotechnology is an emerging scientific field mainly focused on the synthesis and production of various nanomaterials. In particular, nanoparticles' properties may drastically differ from their bulk counterparts, revealing interesting behavior that may be exploited in various applications from medical treatments, batteries for energy storage or clothes. [1],[2] Recently, assembling different materials having various properties, such as hydrophilicity or a surface charge, raised a lot of interest [3],[4]. Indeed, generating anisotropic (objects having different properties in their composing parts) or Janus-like (two different compositions, shape or morphology) particles give rise to unique properties for applications such as dual drug delivery [5], smart textiles [6] or biosensing [7].

In the literature, several methods were reported for the production of anisotropic polymeric nanoparticles (aPNPs) such as emulsion-based method [8], microfluidic approaches [9],[10], masking methods [11] or self-assembly [5]. However, most of these methods imply multistep protocols (e.g. particles' formation followed by surface modification). As an example, aPNPs with a size below 100 nm were produced by Pham *et al. via* reversible addition–fragmentation chain-transfer (RAFT)

polymerization in emulsion. Nanoparticles were composed of two halves of different polymer compositions made of acrylic acid and styrene monomers [11]. However, increasing the number of steps multiplies the risks of contaminations and product loose, hence reducing the productivity. In this context, Lahann's team proposed to produce anisotropic microparticles of poly(ethylene oxide) and poly(acrylic acid) by limiting the number of process steps, using co-jetting with Taylor cone [12]. Later, aPNPs smaller than 150 nm where obtained from an non-emulsion method from poly(lactic-co-glycolic-acid)-poly(ethylene glycol) diblock copolymers [13]. Here, a three-dimensional microfluidic system with a "T" junction was employed to nanoprecipitate the polymers solubilized in a common solvent (acetonitrile) in water. However, since their microfluidic system was made out of poly(dimethyl siloxane), it would not allow the production of oil-in-water emulsions. In 2021, our team also demonstrated the possible way to fabricate Janus PNPs having a chemical anisotropy in a single-step by emulsification-evaporation method [10]. Here, microfluidic-based device was used to produce biodegradable Janus PNPs, with a maximum diameter equal to 250 nm, with a negatively charged hemisphere of poly(styrene sulfonate) and a neutral hemisphere of poly(lactic-co-glycolic acid). [4].

In the present work, various polymers having different hydrophobicity were introduced in an elongational-flow reactor and mixer in order to efficiently produce aPNPs. The chosen macromolecules were poly(styrene sulfonate) (PSS), poly(methyl methacrylate) (PMMA) and poly(lactic-co-glycolic acid) (PLGA) because PSS-PMMA and PSS-PLGA blends had a highly immiscible character due to the huge hydrophobicity difference between the polymers. Precisely, the elaboration of single, blend and Janus PNPs made of PMMA, PLGA and PSS, and their mixtures, were developed *via* the microfluidic-assisted emulsification-evaporation method. Compared to previous works done with PNPs [14]-[16], here the continuous phase pre-saturation method was applied to stabilize the PSS particles.

2. Materials and methods

2.1. Materials

Poly(lactic-co-glycolic acid) 50:50 block copolymer Resomer® RG 504 H (PLGA, Merck, 64,000 g/mol), a linear chain poly(methyl methacrylate) (PMMA, Merck, 120,400 g/mol), poly(styrenesulfonate) (PSS, Sigma, 70,000 g/mol) an anionic polymer, ethyl acetate (Merck) and Pluronic® F-127 (Merck) as a non-ionic surfactant were used as received.

2.2. Preparation of the emulsions

The continuous phase was composed of 1.5 w% of surfactant solubilized in deionized water. When specified, the pre-saturation method was applied, adding 8.7% v/v of ethyl acetate into the former "traditional" continuous phase. The dispersed phase was composed of 1% w/v of the given polymers (PLGA, PMMA or PSS) solubilized in ethyl acetate.

Samples at various continuous/dispersed phases (C/D) volume ratios were emulsified by an elongational-flow reactor and mixer (μRMX) at room temperature. The μRMX consisted in two mid pressure syringe pumps (neMESYS® Mid Pressure Module, Cetoni), two 25 mL stainless steel syringes (Cetoni) and one poly(etheretherketone) tee (Valco Vici). The syringe pumps were connected and operated by the supplier's software in order to operate both pumps at the same reciprocating flow rate. By using this technique, liquid phases can be independently injected or withdrawn. The micromixer was composed of a microchannel of 0.15 mm diameter acting as a restriction to the flow, and linked to the stainless-steel syringes by two poly(tetrafluoroethylene) tubings (1.06 mm ID, 1.68 mm OD). After

emulsification operations, all samples were left overnight in a fume hood to let the polymers' solvent evaporated and the polymer to precipitate forming as such a nanosuspension of solid PNPs in water.

2.3. Characterization methods

2.3.1. Determination of particle size and size distribution

The z-average diameter and size distribution of the PNPs were assessed by dynamic light scattering (DLS) using a Nano ZetaSizer instrument (Malvern) with a helium-neon laser (4 mW, 633 nm). The scatter angle was fixed at 173° and the sample temperature was maintained at 25°C.

The polydispersity index of the particle size (PDI) is a measure of the broadness of the size distribution and it was commonly admitted that PDI values below 0.2 correspond to monomodal distributions [17],[18]. Analyses of nanoparticles diameter were performed by pouring dropwise 0.02 mL of the nanosuspensions into 1 mL of deionized water. Measurements were conducted in triplicates, each measurement being an average of 30 values calculated by the ZetaSizer.

2.3.2. Transmission electron microscopy

To analyze the morphology and shape of the nanoparticles, transmission electron microscopy (TEM) experiments were performed. 5 µL of the nanosuspensions were deposited onto a freshly glow discharged carbon-covered grid (400 mesh). The nanosuspension was left for 2 minutes and then the grid was negatively stained with 5 µL of uranyl acetate (2v% in water) for another minute before being dried using a filter paper. The grids were observed at 200 kV with a Tecnai G2 (FEI) microscope. Images were acquired with an Eagle 2k (FEI) ssCCD camera.

2.3.3. Fourier Transform Infrared

Materials were characterized by the Fourier transform infrared spectroscopy (FTIR, Bruker) to understand if the polymer molecules remained stable or degradation took place during and after the process. Vertex 70 from Bruker Optics was used to record FTIR spectra equipped with MCT (mercury cadmium telluride) detector and a black-body source. The spectra of the solids were measured on diamond through ATR (attenuated total reflectance). Following an intensive purification and lyophilization, prepared PNPs powder was brought to contact with the diamond surface of the FTIR spectroscopy and the measurements were recorded.

3. Results and Discussions

Following the solvent pre-saturation approach, both single PNPs and aPNPs were produced with the elongational-flow reactor and mixer (µRMX) to achieve different nanoparticles' compositions and morphologies.

In the following part, the influence of process parameters (emulsification time, flow rate and microchannel-restriction size) as well as material parameters (continuous/dispersed phase C/D volume ratio, polymers ratio) on the PNPs' diameter and size distribution were assessed. The varied parameters of the µRMX are given in Table 1.

Table 1. Process and material parameters used to produce PNPs.

Emulsification time (min)	Flow rate (mL/min)	C/D volume ratio	Ratio between polymers (w/w)	Microchannel size (µm)
20 to 100†	10 to 50	60/40 and 85/15	100/0 to 0/100	150, 250, 500 and 750

†60 min corresponds to 150 cycles

3.1. Influence of the process parameters

In this part, the results of the influence of the above process parameters (Table 1) were described. The C/D volume ratio and the ratio between polymers were kept constant and respectively equal to 60/40 and 50/50.

A first study has been conducted to produce PMMA-PLGA PNPs (Figure 1), showing that their size and size distribution were directly controlled by the process parameters of the µRMX. Indeed, after a long emulsification time (150 cycles corresponding to 1 h) at 30 mL/min, a near plateau value was obtained at 110 nm, PDI = 0.13 (Figure 1.a). The flow rate itself also affected the PNPs' size, thus above 20 mL/min, the size decreased below 200 nm, PDI ≤ 0.2, and a plateau value was reached above 30 mL/min (Figure 1.b). Interestingly, in Figure 1.c, the microchannel's diameter induced a quite linear variation of highly controlled monomodal (PDI < 0.2) PNPs size ranging from 110 nm (150 µm) to 207 nm (750 µm). To conclude, 150 cycles, flow rate of 30 mL/min, and microchannel's diameter of 150 µm were optimum operating parameters to achieve the minimum PNPs' size (110 nm) and size distribution (PDI = 0.13).

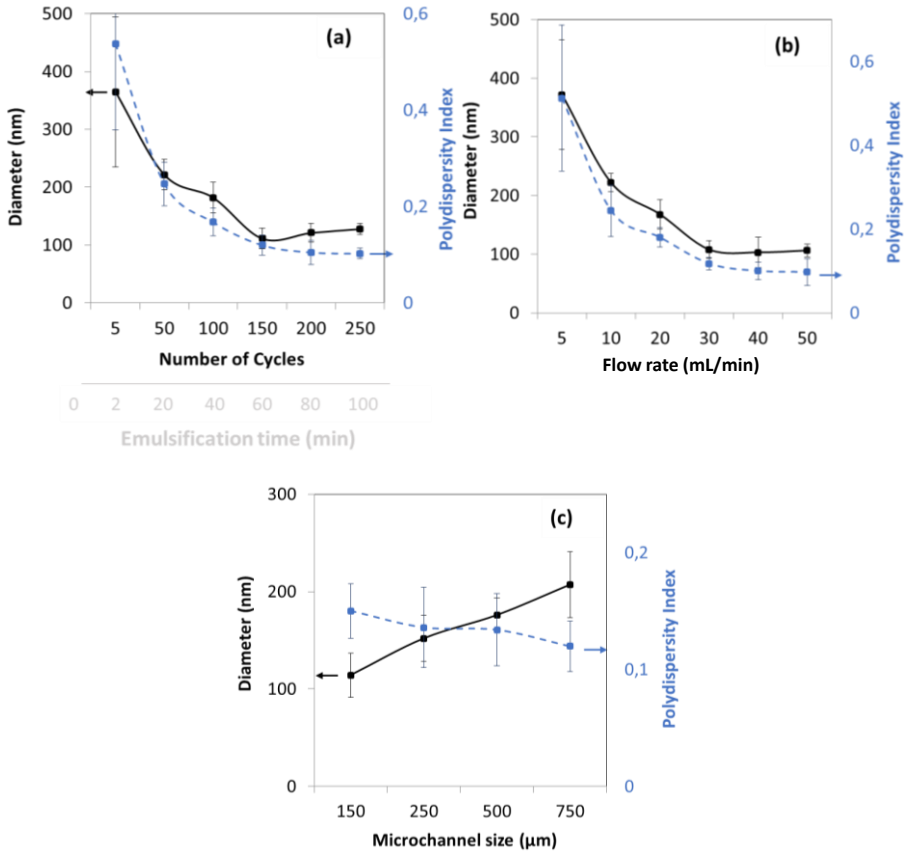

Figure 1. Evolution of PMMA-PLGA (50/50) nanoparticles' size and size distribution at different (a) number of cycles (30 mL/min, microchannel's diameter of 150 µm), (b) flow rates (150 cycles, microchannel's diameter of

150 µm) and (c) microchannel's diameter (30 mL/min, 150 cycles). Experiments were all conducted with the µRMX at 60/40 C/D volume ratios.

The evolution of PMMA-PLGA NPs' diameter and PDI by varying the process parameters followed the same trend than the one obtained from our previous studies on single PLGA and PMMA PNPs [10,19, 20]: at higher elongational strain (*i.e.* a higher flow rate and/or smaller microchannel size) or longer emulsification time, smaller PNPs were produced before reaching a plateau value. This indicates that the introduction of a second polymer in the recipe does not change significantly the trends induced by the variation in process parameters. Moreover, the results for PLGA-PSS (Figure S1) and PMMA-PSS (Figure S2) PNPs were coherent with these observations for aPNPs: only the diameters' values changed not the trend. The optimal process parameters used in the following parts are given in Table 2.

Table 2. Optimal process parameters used to produce aPNPs with the µRMX.

Emulsification time (min)	Flow rate (mL/min)	Microchannel's size (µm)
60	30	150

3.2. Influence of the phases' composition and volume ratio

In this second part, the influence of the C/D volume ratio and the composition of the continuous phase on the PNPs was investigated. The process parameters were given in Table 2 and the ratio between polymers were equal to 50/50. Since the trendline (lower size at higher elongational strain) is the same for single PNPs, PMMA-PLGA, PMMA-PSS, and PLGA-PSS NPs, only the results obtained for PMMA-PLGA blends and single particles were given in Table 3.

Table 3. Evolution of PLGA, PMMA and PMMA-PLGA PNPs' diameter produced at various C/D volume ratios with the µRMX (30 mL/min, 150 cycles, microchannel of 250 µm). Different pre-process conditions were used to compare size differences between traditional and pre-saturated continuous phase.

	Single PLGA NPs' diameter (nm)		Single PMMA NPs' diameter (nm)		PMMA-PLGA NPs' diameter (nm)	
	C/D = 60/40	C/D = 85/15	C/D = 60/40	C/D = 85/15	C/D = 60/40	C/D = 85/15
Continuous phase with Pluronic F127® only	125 ± 7	106 ± 9	140 ± 10	105 ± 8	128 ± 9	105 ± 4
Pre-saturated continuous phase	109 ± 3	96 ± 4	102 ± 5	95 ± 5	110 ± 3	98 ± 5

In Table 3, all three PLGA, PMMA, and PMMA-PLGA NPs showed a similar trend of size: a decrease when the C/D volume ratio increased from 60/40 to 85/15. All results were coherent with previous studies demonstrating that decreasing the polymer concentration, *i.e.* increasing the C/D volume ratio, decreased the system's viscosity, leading to the production of smaller particles. [10,19-21]

Additionally, changing the pre-process condition also reduced the PNPs' size. Indeed, the PMMA-PLGA NPs' size achieved with a C/D phase volume ratio equal to 60/40 was 110 nm (PDI = 0.13) with phase pre-saturation conditions, which corresponds to a size reduction by more than 10% compared to the traditional condition (*i.e.* absence of ethyl acetate in dispersed phase, 128 nm). This reduction may be explained as follows: during the emulsification and in absence of pre-saturation, ethyl acetate diffuses from the droplets to the continuous phase. As such the viscosity of the droplets increases which results, as it was already mentioned in a previous work [22], in bigger nanoparticles. With pre-saturation, the ethyl acetate diffusion is blocked and thus smaller particles are obtained due to lower droplet's viscosity.

Another important novelty was that in pre-saturation conditions, the effect of the C/D phase volume ratio was lessened to only 6% of diameter decrease (from 110 nm to 98 nm, for PMMA-PLGA aPNPs). This was induced by the reduced ethyl acetate diffusion into the water phase at pre-saturation condition compared to the traditional condition.

Overall, following the C/D phase volume ratio optimization, the ratio of 60/40 allowed for achieving an optimum PNPs' size when the pre-saturation condition was maintained.

3.3. Influence on the polymers' ratio

The last crucial parameter influencing the aPNPs' diameter and size distribution is the weight ratio between polymers. This aspect has been deeply investigated for PMMA-PLGA (Figure 2.a), PMMA-PSS (Figure 2.b) and PLGA-PSS (Figure 2.c) systems.

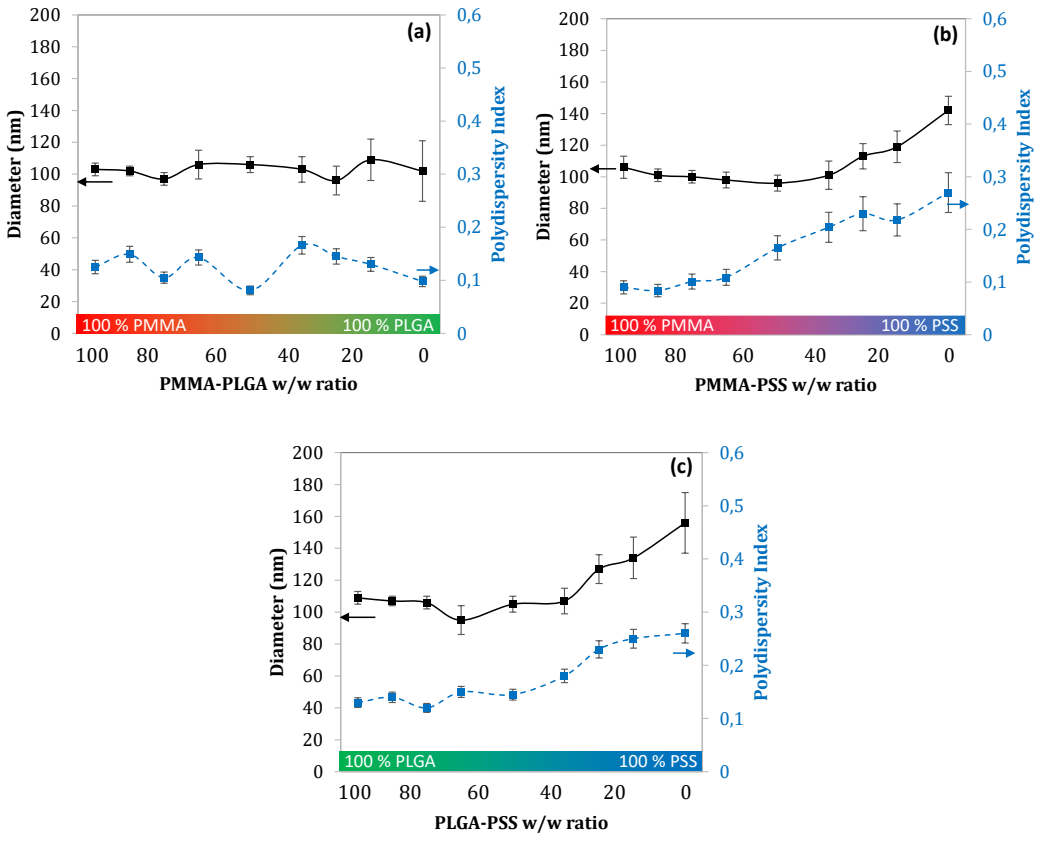

Figure 2. Evolution of the PNPs' size and size distribution at various polymer mass relative percentages for a) PMMA-PLGA, b) PMMA-PSS and c) PLGA-PSS. Experiments were conducted at C/D = 60/40, 150 cycles, 30 mL/min, microchannel's diameter of 150 µm.

Firs of all, PMMA-PLGA blend NPs showed a similar PNP's size around 100 nm at all polymer ratios. This stable value was due to the highly soluble nature of both PLGA and PMMA polymers in ethyl acetate, their low solubility in the aqueous phase and the similar diameter of the PNPs obtained with both single polymers (Table 3).

More interestingly, in Figure 2.b, the PMMA-PSS PNPs' size ranged from 108 nm to 147 nm and the PDI value was ranging from 0.1 to 0.3, depending on PMMA mass relative percentage (0 to 100%). In addition, these particles' sizes were relatively constant around 100 nm until reaching a maximum PSS concentration equal to 80%, where its electronic repulsion and relative hydrophilicity allowed water penetration into the aPNPs, explaining low-control in size. This phenomenon was observed similarly in PLGA-PSS particles (Figure 3.c).

The optimal parameters for process and pre-process are thus summarized in Table 4 and the related DLS size distribution graphs are available in Figure S3.

Table 4. Optimal parameters used to produce PNPs, with the pre-saturation method.

Emulsification time (min)	Flow rate (mL/min)	C/D volume ratio	Ratio between polymers (w/w)	Microchannel's size (µm)
60	30	60/40	65:35	150

3.4. Single, blend and Janus structures

In order to verify the morphology of the aPNPs produced with the µRMX (conditions in Table 4), they were characterized with transmission electronic microscope (Figure 3).

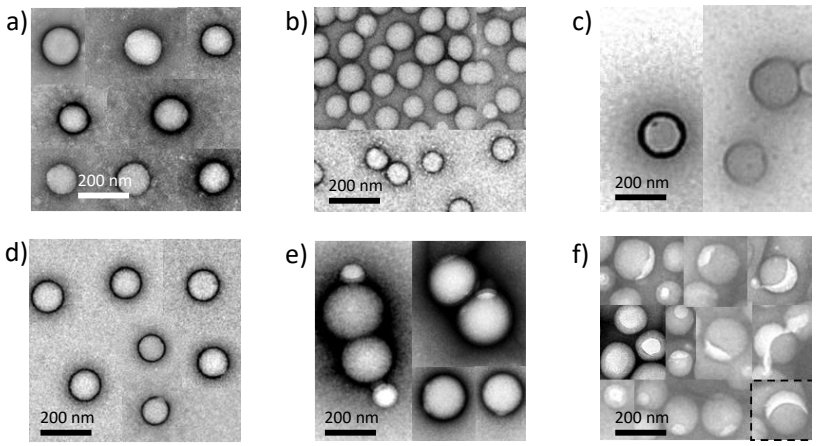

Figure 3. TEM images showing the surface morphology of a) PMMA, b) PLGA, c) PSS, d) PMMA-PLGA, e) PLGA-PSS and f) PMMA-PSS nanoparticles produced with the µRMX (150 cycles, 30 mL/min, microchannel's size 150 µm) with pre-saturation method.

In Figure 3, the single PMMA, PLGA and PSS NPs' diameter were equal to 110 nm, 97 nm and 192 nm respectively with similar spherical shapes, which was coherent with previous DLS results (Table 3, Figure 2). Since PLGA and PMMA were both neutral polymers with approximately the same hydrophobicity and same chemistry, it was not surprising to not see any anisotropy with the PMMA-PLGA particles (Figure 3.d): both polymers were mixed in the particles without clear phase separation.

However, PLGA-PSS and PMMA-PSS aPNPs appeared in the Janus form. This anisotropy was due to the immiscible nature of the charged and neutral polymers, which induced their separation during the organic solvent evaporation. The fact that the smaller and lighter area of these both systems was composed of PSS, previously assessed by cryo-TEM [10], was confirmed in this work (Figure S4). FTIR technique was also used to verify the chemical composition of all the produced nanoparticles (Figure 4).

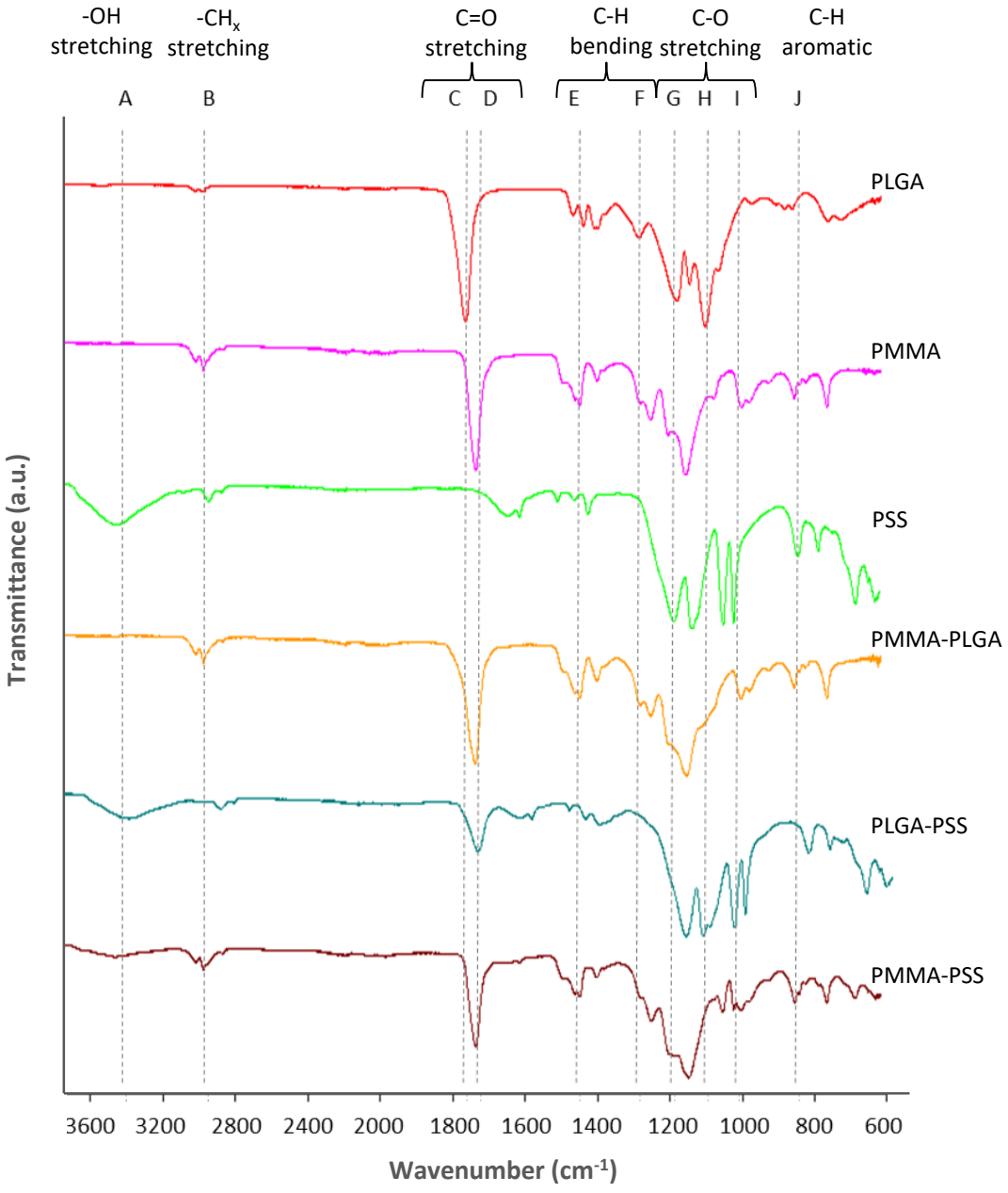

Figure 4. FTIR spectra of the different produced polymeric nanoparticles.

In Figure 4, all the PNPs showed high absorbance in the G-I (1000-1200 cm^{-1}) region representing C-O stretching bonds. PSS showed another high absorbance in J (600-800 cm^{-1}) region, which was not the case in other PNPs, and this can be found in binary-blends containing sulfonate. The region E-F (1300-1500 cm^{-1}), representing C-H bending, was observed in all the samples. The second highly intense absorbance was observed in 1700-1750 cm^{-1} region representing C=O stretching bonds, especially for PMMA (D, 1722 cm^{-1}) and PLGA (C, 1752 cm^{-1}) NPs. This region was wider representing both absorbance points when a blend PMMA-PLGA NPs were measured. In this region PSS did not absorb the IR light, which explains absence of C=O functional groups in PSS molecule. Moreover, in all samples a weak absorbance can be observed representing stretching of $-CH_2$ or $-CH_3$ bonds (B, 2900-3000 cm^{-1}). This analysis was helpful to understand the presence of polymers in PNP blends according to the representing functional groups of each polymer. This analysis also verifies no significant chemical shifts took place while mixing two or more different polymers.

4. Conclusion

This work implemented the emulsification-evaporation method for the one-step production of multi-polymeric components nanoparticles, opening an innovative perspective for the design of new anisotropic PNPs. Indeed, emulsification-evaporation method was a reliable way to achieve both single, binary-blend and even Janus PNPs. In this context, anisotropic NPs were first produced by changing emulsification time, mixing parameters to optimize the system (60 min, 30 mL/min flow rate, and 250 µm microchannel size) in order to achieve minimum values of diameter size and size distribution for PNPs (PDI below 0.2). Following the polymer ratio study, demonstrating the non-monomodality of the systems above the 50% w/w charge/neutral polymers mixing, different PNPs were morphologically characterized and compared. It was revealed that, PMMA-PSS and PLGA-PSS NPs formed a Janus structure with two distinct polymeric parts forming a single spherical matrix, however, PMMA-PLGA NPs were mixed to form single body PNPs matrix. This was correlated with both polymers' hydrophobic nature. This one step production of Janus PNPs method may be suitable for applications such as the co-delivery of two immiscible molecules. Indeed, most of the prepared aPNPs we synthesized out of biocompatible and/or biodegradable polymers.

5. Acknowledgement

The authors would like to thank Mélanie Legros and Marc Schmutz for the access to ICS characterization and electron microscopy platforms respectively. Christian Blanck is acknowledged for the TEM images. Special thanks are addressed to Campus France and French Embassy in Azerbaijan for research funding.

6. Bibliography

[1] H. Mehlhorn, "Nanoparticles – Definitons," In: Mehlhorn, H. (eds) Nanoparticles in the Fight Against Parasites. Parasitology Research Monographs, vol 8. Springer, Cham. doi: 10.1007/978-3-319-25292-

6_1

[2] V. J. Mohanraj, Y. Chen, “Nanoparticles – A review,” Tropical Journal of Pharmaceutical Research, 5 (1), 561-573, 2006. doi: 10.4314/tjpr.v5i1.14634

[3] N. Visaveliya, A. Knauer, W. Yu, C. A. Serra, J. M. Köhler, “Microflow-assisted assembling of multi-scale polymer particles by controlling surface properties and interactions,” Eur. Polym. J., 80, 256–267, 2016, doi: 10.1016/j.eurpolymj.2016.03.015.

[4] M. Vauthier, C. A. Serra, “One-step production of polyelectrolyte nanoparticles,” Polym. Int., 70 (6), 860–865, 2021, doi: 10.1002/pi.6178.

[5] Z. Rahiminezhad, A. M. Tamaddon, S. Borandeh, S. S. Abolmaali, “Janus nanoparticles: New generation of multifunctional nanocarriers in drug delivery, bioimaiging and theranostics,” Appl. Mater. Today, vol. 18, p. 100513, 2020, doi: 10.1016/j.apmt.2019.100513.

[6] S. Saini, B. Kandasubramanian, “Engineered Smart Textiles and Janus Microparticles for Diverse Functional Industrial Applications,” Polym.-Plast. Technol. Mater, 58 (3), 229–245, 2019. doi: 10.1080/03602559.2018.1466177

[7] P. Yánez-Sedeño, S. Campuzano, J. M. Pingarrón, “Janus particles for (bio)sensing,” Appl. Mater. Today, 9, 276–288, 2017, doi: 10.1016/j.apmt.2017.08.004.

[8] S. Ding, C. A. Serra, T. F. Vandamme, W. Yu, N. Anton, “Double emulsions prepared by two–step emulsification: History, state-of-the-art and perspective,” J. Control. Release, 295, 2018, 31–49, 2019, doi: 10.1016/j.jconrel.2018.12.037.

[9] C. Ohm, N. Kapernaum, D. Nonnenmacher, F. Giesselmann, C. A. Serra, R. Zentel, “Microfluidic synthesis of highly shape-anisotropic particles from liquid crystalline elastomers with defined director field configurations,” J. Am. Chem. Soc., 133 (14), 5305–5311, 2011, doi: 10.1021/ja1095254.

[10] M. Vauthier, M. Schmutz, C. A. Serra, “One-step elaboration of Janus polymeric nanoparticles: A comparative study of different emulsification processes,” Colloids Surfaces A Physicochem. Eng. Asp., 626, 127059, 2021, doi: 10.1016/j.colsurfa.2021.127059.

[11] B. T. T. Pham, C. H. Such, B. S. Hawkett, “Synthesis of polymeric janus nanoparticles and their application in surfactant-free emulsion polymerizations,” Polym. Chem., 6 (3), 426–435, 2015, doi: 10.1039/c4py01125b.

[12] K. H. Roh, D. C. Martin, J. Lahann, “Biphasic Janus particles with nanoscale anisotropy,” Nat. Mater., 4 (10), 759–763, 2005, doi: 10.1038/nmat1486.

[13] J. M. Lim, N. Bertrand, P. M. Valencia, M. Rhee, R. Langer, S. Jon, O. C. Farokhzad, R. Karnik, “Parallel microfluidic synthesis of size-tunable polymeric nanoparticles using 3D flow focusing towards *in vivo* study,” Nanomed.: Nanotech. Biol. Med., 10 (2), 401-409, 2014. doi: 10.1016/j.nano.2013.08.003.

[14] S. Ding, M. F. Attia, J. Wallyn, C. Taddei, C. A. Serra, N. Anton, M. Kassem, M. Schmutz, M. Er-Rafik, N. Messaddeq, A. Collard, W. Yu, M. Giordano, T.F. Vandamme, “Microfluidic-Assisted Production of Size-Controlled Superparamagnetic Iron Oxide Nanoparticles-Loaded Poly(methyl methacrylate) Nanohybrids,” Langmuir, 34 (5), 1981–1991, 2018, doi: 10.1021/acs.langmuir.7b01928.

[15] K. Amreen and S. Goel, “Review—Miniaturized and Microfluidic Devices for Automated Nanoparticle Synthesis,” ECS J. Solid State Sci. Technol., 10 (1), 017002, 2021, doi: 10.1149/2162-8777/abdb19.

[16] Y. Singh, J. G. Meher, K. Raval, F. A. Khan, M. Chaurasia, N. K. Jain, M. K. Chourasia, “Nanoemulsion: Concepts, development and applications in drug delivery,” J. Control. Release, 252, 28–49, 2017, doi: 10.1016/j.jconrel.2017.03.008.

[17] S. Ding, N. Anton, T. F. Vandamme, C. A. Serra, “Microfluidic Nanoprecipitation Systems for Preparing Pure Drug or Polymeric Drug Loaded Nanoparticles: An Overview,” Expert Opin. Drug Deliv., 13 (10), 1447–1460, 2016. doi: 10.1080/17425247.2016.1193151

[18] N. Anton, F. Bally, C. A. Serra, A. Ali, Y. Arntz, Y. Mely, M. Zhao, E. Marchioni, A. Jakhmola, T. F. Vandamme, “A New Microfluidic Setup for Precise Control of the Polymer Nanoprecipitation Process and Lipophilic Drug Encapsulation,” Soft Matter., 8 (41), 10628, 2012. doi: 10.1039/C2SM25357G

[19] J. Abdurahim, C. A. Serra, C. Blanck, and M. Vauthier, “One-step production of highly monodisperse size-controlled poly(lactic-co-glycolic acid) nanoparticles for the release of a hydrophobic model drug,” J. Drug Deliv. Sci. Technol., 71, 103358, 2022, doi: 10.1016/j.jddst.2022.103358.

[20] M. Djenouhat, O. Hamdaoui, M. Chiha, M. H. Samar, ‘‘Ultrasonication-assisted preparation of water-in-oil emulsions and application to the removal of cationic dyes from water by emulsion liquid membrane’’, Separation and Purification Technology, 62 (3), 636-641, 2008. doi: 10.1016/j.seppur.2008.03.018.

[21] A. Fetimi, A. Dâas, S. Merouani, A. M. Alswieleh, M. Hamachi, O. Hamdaoui, O. Kebiche-Senhadj, K. K. Yadav, B-H Jeon, Y. Benguerba, ‘‘Predicting emulsion breakdown in the emulsion liquid membrane process: Optimization through response surface methodology and a particle swarm artificial neural

network'', Chem. Eng. And Processing-Process Intens., 176, 108956, 2022, doi: 10.1016/j.cep.2022.108956.

[22] W. Yu, C. A. Serra, I. U. Khan, S. Ding, R. I. Gomez, M. Bouquey, R. Muller, "Development of an Elongational-Flow Microprocess for the Production of Size-Controlled Nanoemulsions: Batch Operation," Macromolecular Reaction Eng., 11 (1), 1600024, 2016. doi: 10.1002/mren.201600024.